Prospects for sub-micron solid state nuclear magnetic resonance imaging with low-temperature dynamic nuclear polarization

ARTICLE *in* PHYSICAL CHEMISTRY CHEMICAL PHYSICS · JUNE 2010

Impact Factor: 4.49 · DOI: 10.1039/c0cp00157k · Source: PubMed

2 AUTHORS, INCLUDING:

Kent Thurber
The National Institute of Diabetes and Digest…

53 PUBLICATIONS **1,256** CITATIONS

SEE PROFILE

Published in final edited form as:
Phys Chem Chem Phys. 2010 June 14; 12(22): 5779–5785. doi:10.1039/c0cp00157k.

Prospects for Sub-Micron Solid State Nuclear Magnetic Resonance Imaging with Low-Temperature Dynamic Nuclear Polarization

Kent R. Thurber and **Robert Tycko***
Laboratory of Chemical Physics, National Institute of Diabetes and Digestive and Kidney Diseases, National Institutes of Health, Bethesda, Maryland 20892-0520

Summary

We evaluate the feasibility of ^{1}H nuclear magnetic resonance (NMR) imaging with sub-micron voxel dimensions using a combination of low temperatures and dynamic nuclear polarization (DNP). Experiments are performed on nitroxide-doped glycerol/water at 9.4 T and temperatures below 40 K, using a 30 mW tunable microwave source for DNP. With DNP at 7 K, a 0.5 μl sample yields a ^{1}H NMR signal-to-noise ratio of 770 in two scans with pulsed spin-lock detection and after 80 db signal attenuation. With reasonable extrapolations, we infer that ^{1}H NMR signals from 1 μm^3 voxel volumes should be readily detectable, and voxels as small as 0.03 μm^3 may eventually be detectable. Through homonuclear decoupling with a frequency-switched Lee-Goldburg spin echo technique, we obtain 830 Hz ^{1}H NMR linewidths at low temperatures, implying that pulsed field gradients equal to 0.4 G/d or less would be required during spatial encoding dimensions of an imaging sequence, where d is the resolution in each dimension.

Introduction

High-field dynamic nuclear polarization (DNP) for applications in solid state nuclear magnetic resonance (NMR) spectroscopy has been developed principally by Griffin and coworkers,[1, 2] following earlier work at lower fields by Schaefer,[3] Yannoni,[4] and Wind.[5] We have recently described a DNP system for solid state NMR at 9.39 T that uses a relatively inexpensive, compact, and tunable source to produce 30 mW microwaves at 264 GHz.[6] With this system, enhancements of ^{1}H nuclear spin polarizations by factors of 80 or more can be achieved at temperatures below 20 K (relative to equilibrium polarizations at the same temperatures) in glycerol/water mixtures with appropriate nitroxide radical dopants. In this paper, we investigate whether sensitivity enhancements from low-temperature DNP might permit solid state NMR imaging with sub-micron spatial resolution. Specifically, we evaluate the absolute sensitivity of DNP-enhanced ^{1}H NMR measurements on sub-microliter samples and the ^{1}H NMR linewidths that can be achieved with simple homonuclear decoupling techniques under DNP conditions. Absolute sensitivity and linewidths are the two primary factors that dictate spatial resolution in NMR imaging, since the sensitivity must be high enough to permit detection of signal contrast from a single voxel in the image and the lines must be narrow enough to permit signals from adjacent voxels to be resolved spectroscopically in the presence of realistic magnetic field gradients. The main conclusions from the experimental results presented below are that ^{1}H NMR imaging with 1 μm^3 voxel volumes should be readily achievable with low-temperature DNP at 9.39 T, and that imaging with 0.03 μm^3 voxels (*e.g.*, cubic volumes, 300

*corresponding author: Dr. Robert Tycko, National Institutes of Health, Building 5, Room 112, Bethesda, MD 20892-0520, phone 301-402-8272, fax 301-496-0825, robertty@mail.nih.gov.

nm on each side) may be achievable with significant effort. These conclusions are interesting because the minimum voxel volumes in inductively-detected NMR images demonstrated to date, through measurements of liquid state ^{1}H NMR signals at ambient temperatures,[7, 8] are roughly 40 μm^3. Thus, imaging at low temperatures with DNP may be a more successful approach in studies relevant to cell biology.

Methods

DNP/NMR apparatus and sample

Our DNP spectrometer has been described previously,[6] Briefly, frequency-tunable microwaves at 264 ± 5 GHz are supplied by a synthesizer-based source (Virginia Diodes, Inc., Charlottesville, Virginia, U.S.A.), polarized by a quasi-optical system (Thomas Keating, Ltd., West Sussex, U.K.), and transmitted vertically upwards through the bore of a 9.39 T superconducting NMR magnet by a section of corrugated waveguide. The microwave power is nominally 30 mW. At the end of the waveguide, a corrugated horn mates with a high-density polyethylene window at the bottom of a modified Janis SuperTran continuous flow cryostat. The cryostat has a “cold finger in vacuum” design that, in principle, permits measurements over a temperature range from below 4.2 K to 300 K. Microwaves traverse the window and are transmitted through a brass tube (30 mm length, 3.2 mm inner diameter) to the radio-frequency (RF) coil of our NMR probe circuit within the cryostat.

Figure 1 shows relevant parts of the cryostat, RF circuit, and sample holder. For the experiments described below, the RF coil consists of six turns of 0.2 mm-diameter copper wire, wrapped around a section of Teflon tubing with 1.2 mm outer diameter. The coil is 3.0 mm in length, leaving 0.35 mm gaps between windings through which the microwaves pass. The sample is centered in the coil, contained in a space between two sapphire rods (Swiss Jewel Co., Philadelphia, Pennsylvania, U.S.A.) that fit snugly in the Teflon tubing. A vacuum seal is produced by clamping the Teflon tubing to the sapphire rods with wire. The sapphire rods insert into copper plates that are thermally sunk to the temperature-controlled copper cold finger of the cryostat. The sapphire rods provide the thermal contact between the sample and the cold finger, and are attached to the copper plates with vacuum grease and set screws.

The RF coil is grounded at one end. Tuning and matching to 50 Ω at the ^{1}H NMR frequency (400.9 MHz) is achieved by a 3.6 pf ceramic chip capacitor (American Technical Ceramics, Huntington Station, New York, U.S.A.) soldered directly across the coil and by variable series tuning and parallel matching capacitors (Polyflon Co., Norwalk, Connecticut, U.S.A.) that are located within the cryostat’s radiation shield, with a distance of approximately 2.5 cm between the tuning capacitor and the RF coil. Pistons in the variable capacitors are reduced in diameter to prevent binding at low temperatures.

The cryostat contains a field modulation coil, positioned around the RF coil, that produces a 5.0 G/A field parallel to the main field of the NMR magnet. As previously described, the modulation coil is used for EPR spectroscopy and for enhancement of DNP.[6] In the experiments described below, the modulation coil is used to produce pulsed direct-current (DC) fields that test our ability to resolve NMR frequency shifts during homonuclear decoupling. For this purpose, a simple transistor switching circuit, under control of the spectrometer’s pulse programmer, generates current pulses up to 300 mA with a 2 μs switching time. With the current cryostat configuration, eddy currents in the copper components within the modulation coil reduce the pulsed fields at the sample to 3.4 G/A. At low temperatures, the eddy currents persist for times that greatly exceed the durations of the DC field pulses in experiments described below. The modulation coil can also act as an antenna for sensing the amplitude and phase of RF fields (see below).

Experiments were performed on 0.5 μl samples of glycerol/water (1:3 molar ratio), containing 220 mM acetate buffer (pH 3) and either 5 mM or 30 mM DOTOPA-TEMPO, a trinitroxide radical dopant that we have recently introduced for low-temperature DNP.[6] At low temperatures and under DNP, ^{1}H NMR signals from these samples are so strong that they must be attenuated by as much as 80 db to avoid overloading the receiver of our Varian Infinity NMR spectrometer. All DNP measurements described below were performed with the full available microwave power. The microwave frequency was set to 264.0 GHz, corresponding to the maximum DNP enhancement.

Pulse sequences

Figure 2 shows the pulse sequence used to obtain data discussed below. This sequence is designed to remove the effects of strong ^{1}H-^{1}H magnetic dipole-dipole couplings that otherwise reduce both the sensitivity and the resolution of the measurements. To improve sensitivity, ^{1}H NMR signals are detected with pulsed spin-locking[9] (PSL), which extends the signal decay in the t_2 period by factors of 40–80 (see below). Our PSL detection technique consists of a train of short, high-power RF pulses (1.5 μs lengths, 270 kHz amplitude) separated by 8.2 μs delays. The average RF amplitude during PSL is therefore 42 kHz. After each PSL pulse, six complex signal points are digitized with a 1.0 μs dwell time. A 2.0 μs ring-down delay precedes digitization of the first signal point.

In the t_1 period, homonuclear dipole-dipole couplings and chemical shifts are averaged out coherently by a frequency-switched Lee-Goldburg spin echo technique.[10] This consists of alternating periods of irradiation with the RF carrier frequency shifted by either $+f_{LG}$ or $-f_{LG}$ from the on-resonance condition, with RF phase of either × or −x (+LG and −LG periods in Figure 2). The RF amplitude is 149 kHz, so that f_{LG} = 105 kHz produces an effective field in the rotating frame at the "magic angle" $\theta_m=\cos^{-1}(1/\sqrt{3})$ with 182 kHz amplitude. An RF pulse with flip angle $\pi/2$-θ_m before the t_1 period rotates the ^{1}H spin magnetization from the rotating frame z axis to a direction perpendicular to the effective field. A pulse with flip angle θ_m after the t_1 period rotates the magnetization to the xy plane. Alternation between +LG and −LG ensures that the effective field produces no net precession for on-resonance spins. Spins that are off-resonance due to isotropic and anisotropic chemical shifts experience a non-zero net precession in each $t_1/2$ period, but this precession is refocused by the π pulse in the middle of the Lee-Goldburg period. Application of a DC field pulse in either the first or the second half of the t_1 period produces a net precession that is not refocused. Thus, the signal decay with respect to t_1 in the absence of dc field pulses indicates the homogeneous linewidth under Lee-Goldburg decoupling. Oscillations with respect to t_1 in the presence of DC field pulses indicate precession that would be spatially-dependent in an imaging experiment with pulsed field gradients.

Real and imaginary signal (*i.e.*, x and y magnetization) components at the end of t_1 are detected by using PSL pulses with either x or y phase. In addition, a π pulse is applied 1 ms before the Lee-Goldburg period on alternate scans and NMR signals are alternately added or subtracted to cancel baseline offsets, background signals, and residual ring-down from the PSL pulses. Our implementation of PSL does not require an increase in the spectrometer's receiver bandwidth beyond the value used without PSL.

Because the values of f_{LG} are not negligibly small compared with the width of the NMR probe circuit's resonance, shifts in the RF carrier frequency alter the amplitudes and phases of RF fields at the sample. We directly measure these amplitudes and phases by mixing the RF signals picked up by the field modulation coil during the pulse sequence with the output of a frequency synthesizer (set to the RF carrier frequency at the on-resonance condition) and viewing the output of the mixer on an oscilloscope, after low-pass filtering. Oscilloscope traces verify that

frequency switching occurs in a phase-continuous manner with our Varian Infinity spectrometer (as required for successful implementation of frequency-switched Lee-Goldburg decoupling), with switching times of approximately 300 ns. The x and −x RF phases in the +LG and −LG periods require adjustments by approximately ±8° to produce the required phases at $\pm f_{LG}$ offsets. Adjustments of the RF circuit tuning to approximately match the reflected power at $\pm f_{LG}$ offsets and adjustments of the RF amplitudes by approximately 2% are performed to balance the effective fields in the +LG and −LG periods. Final optimization of Lee-Goldburg decoupling is carried out by adjusting $|f_{LG}|$ and the RF amplitude during −LG periods to produce the slowest possible signal decay with respect to t_1 in the absence of DC field pulses.

Results

NMR sensitivity

Figures 3a–3d show ^{1}H free-induction decay (FID) signals from 0.5 μl glycerol/water samples, with and without PSL. Fourier transforms are shown in Figures 3e–3h. Without PSL, the signal decays to 50% of its initial amplitude in 7.0 μs, or 7 signal points with a 1.0 μs dwell. With PSL, the signal decays to 50% of its initial amplitude in 240 points with 30 mM DOTOPA-TEMPO or 410 points with 5 mM DOTOPA-TEMPO. The dependence on paramagnetic dopant concentration is apparently due to a nuclear T_2 relaxation process that involves the dopant. PSL decay times are not significantly different at 7 K and 35 K, indicating that this process is temperature-independent. Fluctuations of local hyperfine fields due to electron-electron couplings or electron spin diffusion are a likely source of the nuclear spin T_2.

Signal-to-noise ratios (SNR) are approximately proportional to $\sqrt{N_{1/2}}$, where $N_{1/2}$ is the number of signal points for 50% decay. Thus, PSL enhances the SNR for detection of ^{1}H NMR signals by a factor of 6–8. The number of scans required to achieve a given SNR is proportional to $N_{1/2}$, and is reduced by a factor of 34–60.

Figure 4 shows the growth of ^{1}H NMR signal amplitudes after initial saturation by a train of RF pulses. At 35 K, ^{1}H T_1 relaxation (without microwaves) and DNP build-up times are both equal to 1.85 ± 0.10 s with 30 mM DOTOPA-TEMPO and 43.0 ± 1.5 s with 5 mM DOTOPA-TEMPO. With 30 mM DOTOPA-TEMPO at 7 K, the T_1 relaxation time is 10.6 s, while the DNP build-up time is 3.6 s. We attribute the differences between T_1 relaxation and DNP build-up times at 7 K to microwave-induced sample heating, due to insufficient thermal conduction from the sample to the cryostat's cold finger. Microwave irradiation at frequencies outside the EPR lineshape does not affect the ^{1}H T_1, indicating that sample heating results from resonant microwave absorption by electron spins.

With 5 mM DOTOPA-TEMPO, ^{1}H NMR signals are enhanced by a factor of 16 at 35 K. With 30 mM DOTOPA-TEMPO, NMR signal amplitudes are enhanced by factors of 40 and 75 at 35 K and 7 K, respectively. The largest signals are observed with 30 mM DOTOPA-TEMPO at 7 K. The absolute SNR is defined by

$$\mathrm{SNR}=\frac{\sum_{i=1}^{N} s_i a_i}{\nu_{\mathrm{rms}}\sqrt{\sum_{j=1}^{N} a_j^{\,2}}} \qquad (1)$$

where N is the number of signal points in the FID, s_i is the signal at the i^{th} point, ν_{rms} is the root-mean-squared noise at each point, and a_i is the value of an apodization function at the i^{th} point. SNR is maximized with "matched filtering", *i.e.*, when a_i is proportional to s_i.[11] Assuming that N does not greatly exceed the value at which the signal decays to the noise level, Eq. (1) becomes

$$\mathrm{SNR} \approx \frac{1}{\nu_{\mathrm{rms}}} \sqrt{\sum_{i=1}^{N} s_i^2} \tag{2}$$

Using Eq. (2), the absolute SNR in our experiments at 7 K with 30 mM DOTOPA-TEMPO and with PSL is 770 after two scans. Taking into account the 80 db attenuation before the spectrometer's receiver (see above), the absolute SNR without attenuation would be 1.0 after one scan for a sample volume of 90 femtoliters, or $(4.5\ \mu m)^3$.

We use Eq. (2) to determine the SNR from the time-domain signals rather than measuring the SNR in the frequency domain after Fourier transformation because signals were not sampled in constant time increments under PSL and because the time-domain signals contain periodic ring-down glitches (see Fig. 3b and 3d). It is therefore difficult to determine the noise level accurately from the Fourier transformed signals.

Spectral resolution

Figure 5a shows the dependence of ^1H NMR signals on t_1, using the pulse sequence in Figure 2. Without DC field pulses, the dependence on t_1 is approximately Gaussian, with a 1/e decay time of 630 μs with 5 mM DOTOPA-TEMPO, corresponding to a nearly Gaussian lineshape with 830 Hz full-width at half-maximum (FWHM). Compared with the 80 kHz FWHM observed in the absence of homonuclear decoupling (see Figure 3g), the frequency-switched Lee-Goldburg spin echo technique in Figure 2 produces line-narrowing by a factor of nearly 100.

With DC field pulses, the signals oscillate as a function of t_1. Fourier transformation of the complex signals with respect to t_1 produces the lineshapes in Figure 5b. Application of a 0.91 G field (including eddy current effects) during half of the t_1 period shifts the NMR line by 1.02 kHz (*i.e.*, 1.23 times the FWHM), in good agreement with the 1.12 kHz shift predicted from the DC field strength and the theoretical $0.5\times3^{-1/2}$ scaling factor for the pulse sequence in Figure 2. The small discrepancy between the observed and predicted shift is likely due to uncertainty in our calibration of eddy currents. If the DC field is reversed, the shift is also reversed as expected.

If field pulses were applied in both halves of t_1, but with opposite polarity, 0.37 G fields would be sufficient to shift the NMR line by an amount equal to its FWHM. Thus, an NMR imaging experiment would require field gradients approximately equal to 0.4 G/d, where d is the spacing between voxels in one dimension.

At 30 mM DOTOPA-TEMPO, the 1/e time with respect to t_1 decreases to 160 μs and the signal decay is approximately single-exponential, rather than Gaussian (data not shown). Lineshapes in t_1 are then nearly Lorentzian, with 2.1 kHz FWHM. Similar effects on PSL decays are mentioned above. Again, we attribute the more rapid decay in t_1 at higher dopant concentrations to fluctuations of local hyperfine fields due to electron-electron couplings or electron spin diffusion. Since higher dopant concentrations also lead to larger DNP enhancements and more rapid DNP build-up, larger field gradients may permit more rapid acquisition of images with small voxels.

Discussion

A prerequisite for NMR imaging is that the signals from each resolved volume element (*i.e.*, each voxel) be detectable within the total image acquisition time. More precisely, signal variations among different voxels should be detectable with statistical significance. If a SNR ratio of 1.0 is obtained for a volume v_1 in one scan in a one-dimensional NMR measurement, the time between scans is t_s, the total acquisition time is T_{tot}, and the fractional signal variations among voxels (*i.e.*, the contrast) is c, then the minimum voxel size v_{min} is

$$v_{min} = \Theta \frac{v_1 t_s^{1/2}}{c T_{tot}^{1/2}} \quad (3)$$

where Θ is a factor that includes the desired statistical significance and accounts for signal losses from transverse spin relaxation during the indirect dimensions of the multidimensional imaging measurement. With $\Theta \approx 10$, $c \approx 0.5$, and $t_s/T_{tot} \approx 1 \times 10^{-4}$ (corresponding to a 24 hr image time with $t_s = 8.6$ s), Equation (3) yields $v_{min} = 0.2v_1$. In the experiments described above, v_1 is 90 femtoliters, implying $v_{min} = (2.6\ \mu m)^3$. This volume could be reduced by several obvious improvements: (a) Our NMR spectrometer is far from being optimized for ^{1}H NMR detection. The receiver noise temperature at the ^{1}H NMR frequency is 390 K (3.7 db noise figure), as measured at the input to the probe circuit using a calibrated noise source. Improvements to the transmit/receive switching network and use of a cooled preamplifier[12] may reduce the noise voltage by a factor of 3–6; (b) Our RF coil is much larger than needed for sub-microliter samples. Reducing the coil volume by a factor of 10–100 may increase the signals by a factor of 3–10; (c) In principle, DNP enhancements of ^{1}H spin polarizations can be increased by a factor of 8 through higher microwave power densities and further developments in paramagnetic dopants. Lower sample temperatures would also permit larger absolute polarizations. Combining these improvements, a reduction in v_{min} by a factor of 500, to approximately $(0.3\ \mu m)^3$, seems feasible. Thus, sub-micron solid state NMR imaging at low temperatures with DNP enhancement is a reasonable goal from the sensitivity standpoint.

A second prerequisite for NMR imaging is that magnetic field gradients be large enough to make the NMR frequencies of adjacent voxels resolvable. Using the frequency-switched Lee-Goldburg spin echo technique in Figure 2, we have achieved homogeneous ^{1}H NMR linewidths of 830 Hz. Voxel dimensions in the 0.3–2.6 μm range therefore require field gradients in the 130–1100 G/mm range (including the $\sqrt{3}$ reduction in gradient-induced frequency shifts due to projection onto the Lee-Goldburg effective field). Gradient coils and power supplies for micro-imaging that produce 150 G/mm pulsed field gradients have been described by Pennington and coworkers.[13, 14] Larger gradients can in principle be achieved by reducing the dimensions of the gradient coils. Smaller homogeneous linewidths may be achieved by using more elaborate homonuclear decoupling sequences.[15] Thus, although many engineering challenges remain, sub-micron solid state NMR imaging at low temperatures is not precluded by a requirement for impossibly large field gradients.

Pennington and coworkers have reported ambient-temperature ^{1}H NMR imaging at 9.0 T with 3.7 μm × 3.3 μm × 3.3 μm voxels.[8] In their experiments, high sensitivity was achieved with a combination of RF microcoils (73 μm diameter), Carr-Purcell echo train detection, and paramagnetic doping to produce rapid spin-lattice relaxation and permit a short recycle delay. The low-temperature approach described above has reduced sensitivity because of the larger detected linewidths (0.5–1.0 kHz with PSL detection at low temperature vs. 6 Hz with Carr-Purcell detection at ambient temperature) and longer recycle delays (5–50 s at low temperatures vs. 0.5 s at ambient temperature). However, the resulting sensitivity reduction by a factor 30–130 is more than overcome by a 3000-fold increase in ^{1}H spin polarization with low-

temperature DNP. In principle, even larger DNP effects[1] and a lower receiver noise temperature[12] would make the low-temperature approach clearly advantageous from the standpoint of sensitivity.

The smaller intrinsic NMR linewidths at ambient temperature might permit the use of smaller pulsed field gradients. However, as discussed by Pennington and coworkers,[14] translational diffusion at ambient temperatures requires that gradients of order 120 G/mm be employed to achieve 1 μm spatial resolution. At low temperatures, translational diffusion is quenched. As demonstrated above, homonuclear decoupling techniques can easily reduce the low-temperature linewidths to the point where 1 μm spatial resolution requires 400 G/mm gradients. Thus, field gradient requirements in low-temperature ^{1}H NMR imaging are somewhat more demanding, but only by a factor less than four.

Images with much higher resolution have been obtained by force-detected magnetic resonance.[16] Force detection has been estimated to become more sensitive than inductive detection at sample dimensions below 200 μm.[17] For some applications in cell biology, overall sample dimensions are expected to be on the order of 100 μm (*e.g.*, collections of 10 μm-diameter cells immersed in fluid). The spatial resolution and sensitivity of force-detected imaging decreases with increasing sample depth, making it difficult to image objects within containers or far below the sample surface. Therefore, we expect inductively-detected imaging to be the preferred method for studies of groups of cells and larger objects. Force-detected methods are preferable for viruses, protein assemblies, isolated subcellular components, and similar objects.

Finally, the ability to differentiate among various objects and regions within an image depends on the existence of contrast mechanisms. One can imagine a number of mechanisms in low-temperature NMR imaging of biological samples with DNP. Intrinsic variations in ^{1}H densities may be too small to produce useful contrast by themselves, but local ^{1}H-^{1}H dipole-dipole coupling strengths may vary significantly. For example, nearest-neighbor dipole-dipole couplings in the methylene groups of proteins and lipids are roughly 70% of those in water. Weighting of ^{1}H NMR signals according to local coupling strengths, using appropriate RF pulse sequences, may then produce spatial contrast. Partial deuteration or other isotopic labeling schemes could be employed to generate contrast. Variations in local concentrations of paramagnetic species, including the DNP polarizing agent, other extrinsic dopants, and intrinsic paramagnetic centers, could produce variations in local ^{1}H spin polarizations through variations in DNP enhancements or nuclear spin relaxation rates. Evaluation of these potential contrast mechanisms and explorations of potential applications for DNP-enhanced NMR imaging will be subjects of future work.

Acknowledgments

This work was supported by the Intramural Research Program of the National Institute of Diabetes and Digestive and Kidney Diseases of the National Institutes of Health, and by the Intramural AIDS Targeted Antiviral Program of the National Institutes of Health.

References

1. Maly T, Debelouchina GT, Bajaj VS, Hu KN, Joo CG, Mak-Jurkauskas ML, Sirigiri JR, van der Wel PCA, Herzfeld J, Temkin RJ, Griffin RG. J. Chem. Phys 2008;128:052211. [PubMed: 18266416] Hu KN, Song C, Yu HH, Swager TM, Griffin RG. J. Chem. Phys 2008;128:052302. [PubMed: 18266419] Song CS, Hu KN, Joo CG, Swager TM, Griffin RG. J. Am. Chem. Soc 2006;128:11385–11390. [PubMed: 16939261]
2. Bajaj VS, Hornstein MK, Kreischer KE, Sirigiri JR, Woskov PP, Mak-Jurkauskas ML, Herzfeld J, Temkin RJ, Griffin RG. J. Magn. Reson 2007;189:251–279. [PubMed: 17942352] Farrar CT, Hall

DA, Gerfen GJ, Inati SJ, Griffin RG. J. Chem. Phys 2001;114:4922–4933.Becerra LR, Gerfen GJ, Temkin RJ, Singel DJ, Griffin RG. Phys. Rev. Lett 1993;71:3561–3564. [PubMed: 10055008]

3. Afeworki M, McKay RA, Schaefer J. Macromolecules 1992;25:4084–4091.
4. Singel DJ, Seidel H, Kendrick RD, Yannoni CS. J. Magn. Reson 1989;81:145–161.
5. Wind RA, Hall RA, Jurkiewicz A, Lock H, Maciel GE. J. Magn. Reson. A 1994;110:33–37.Wind RA, Duijvestijn MJ, Vanderlugt C, Manenschijn A, Vriend J. Prog. Nucl. Magn. Reson. Spectrosc 1985;17:33–67.
6. Thurber KR, Yau W-M, Tycko R. J. Magn. Reson. 2010 in press.
7. Ciobanu L, Pennington CH. Solid State Nucl. Magn. Reson 2004;25:138–141. [PubMed: 14698400]
8. Ciobanu L, Seeber DA, Pennington CH. J. Magn. Reson 2002;158:178–182. [PubMed: 12419685]
9. Suwelack D, Waugh JS. Phys. Rev. B 1980;22:5110–5114.Ostroff ED, Waugh JS. Phys. Rev. Lett 1966;16:1097–1098.Petkova AT, Tycko R. J. Magn. Reson 2002;155:293–299. [PubMed: 12036340]
10. Lee M, Goldburg WI. Phys. Rev 1965;140:A1261–A1271.Bielecki A, Kolbert AC, Levitt MH. Chem. Phys. Lett 1989;155:341–346.
11. Ernst, RR.; Bodenhausen, G.; Wokaun, A. Principles of Nuclear Magnetic Resonance in One and Two Dimensions. New York: Oxford University Press; 1987.
12. Styles P, Soffe NF, Scott CA, Cragg DA, Row F, White DJ, White PCJ. J. Magn. Reson 1984;60:397–404.
13. Seeber DA, Hoftiezer JH, Pennington CH. Concepts Magn. Reson 2002;15:189–200.
14. Seeber DA, Hoftiezer JH, Daniel WB, Rutgers MA, Pennington CH. Rev. Sci. Instrum 2000;71:4263–4272.
15. Kempf JG, Miller MA, Weitekamp DP. Proc. Natl. Acad. Sci. U.S.A 2008;105:20124–20129. [PubMed: 19104070] Cory DG, Miller JB, Turner R, Garroway AN. Mol. Phys 1990;70:331–345.
16. Degen CL, Poggio M, Mamin HJ, Rettner CT, Rugar D. Proc. Natl. Acad. Sci. U.S.A 2009;106:1313–1317. [PubMed: 19139397] Thurber KR, Harrell LE, Smith DD. J. Magn. Reson 2003;162:336–340. [PubMed: 12810017]
17. Leskowitz GM, Madsen LA, Weitekamp DP. Solid State Nucl. Magn. Reson 1998;11:73–86. [PubMed: 9650792]

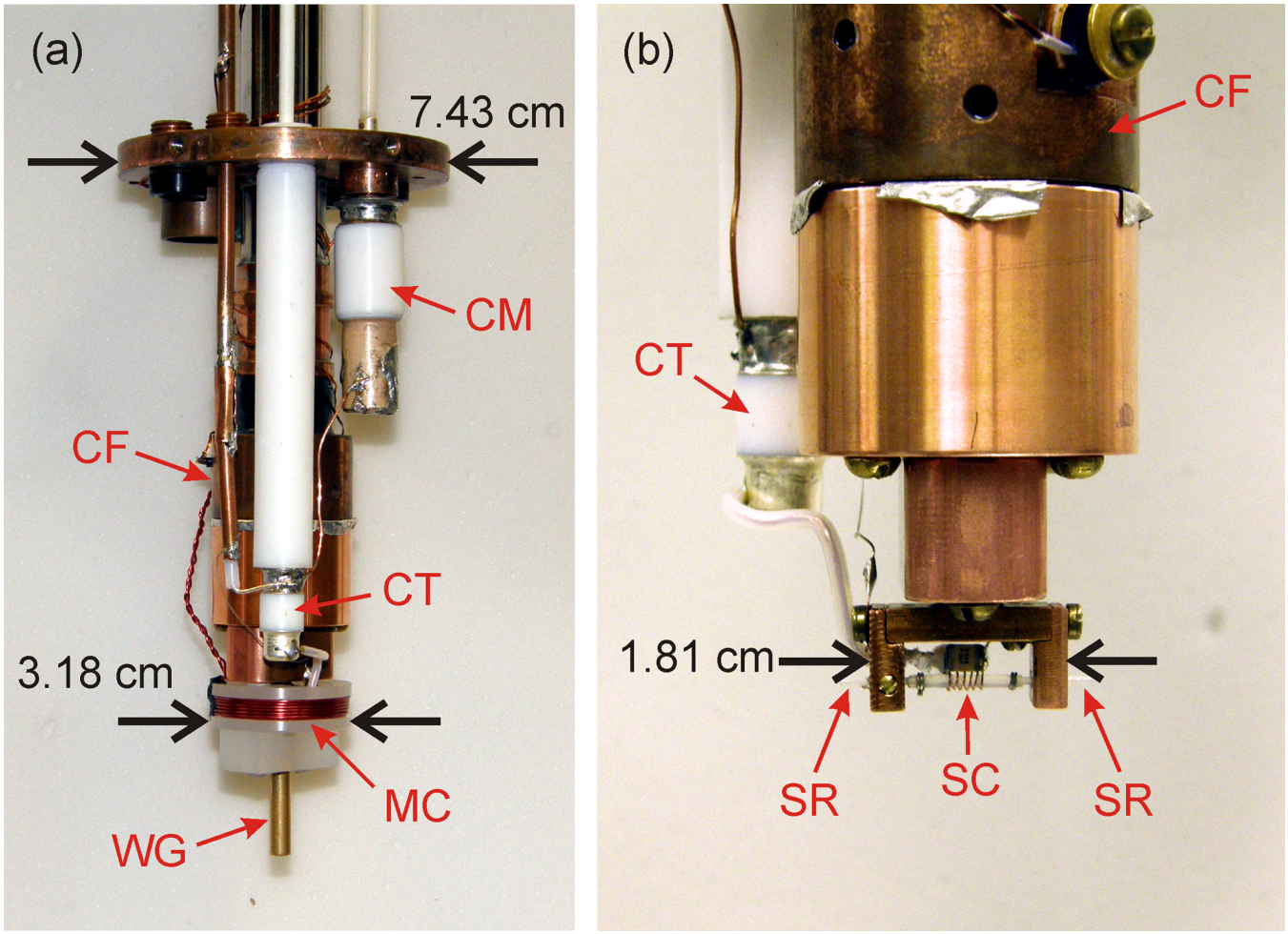

Figure 1.

Photographs of the cryostat head used in low-temperature ^{1}H NMR measurements with DNP. (a) View with modulation coil on Kel-F plastic support (MC) and brass waveguide (WG) in place. Tuning and matching capacitors for the RF resonant circuit (CT and CM, respectively) and temperature-controlled copper cold finger (CF) are also indicated. All of these components are contained within a thermal radiation shield and within an outer vacuum can when the cryostat is in operation. (b) View with the modulation coil removed, showing the RF sample coil (SC). A ceramic chip capacitor behind the coil increases its effective inductance. The glycerol/water sample is contained in a Teflon tube within the coil and thermally sunk to the cold finger through two sapphire rods (SR) that create a 0.5 μl sample volume within the Teflon tube.

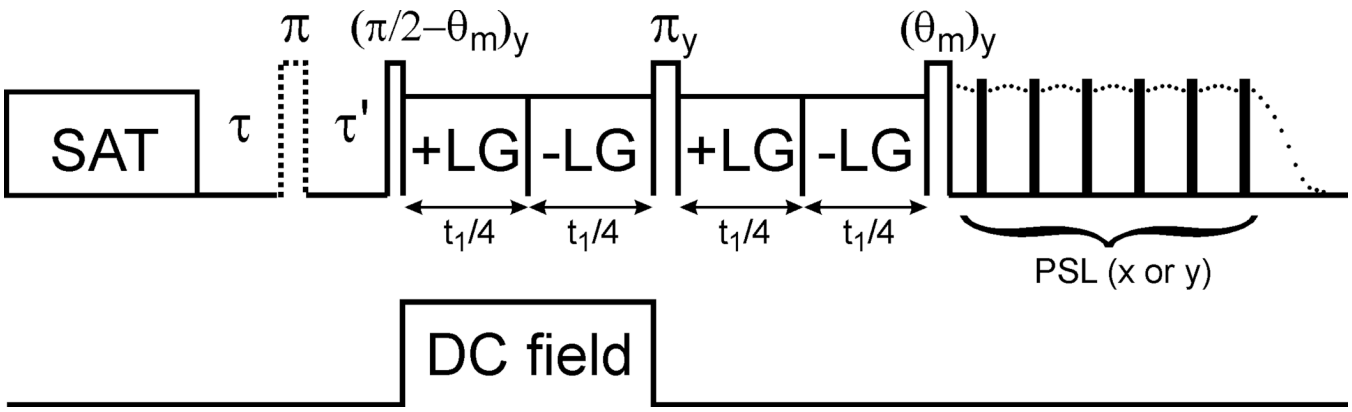

Figure 2.

Pulse sequence for measurements in Figures 3 and [5]. SAT represents a train of RF pulses that saturates (*i.e.*, destroys) pre-existing ^{1}H spin polarization. Polarization builds up during the period τ on the time scale of 1–100 s, either towards its thermal equilibrium value if microwaves are not applied or towards a DNP-enhanced value if microwaves are applied. A π pulse on alternate scans, with alternate addition and subtraction of NMR signals, suppresses both RF ring-down and ^{1}H NMR signals from material outside the RF coil. After the 1 ms delay τ', a frequency-switched Lee-Goldburg spin echo sequence removes ^{1}H-^{1}H dipole-dipole couplings and chemical shifts during the evolution period t_1, with +LG or −LG representing off-resonance irradiation with a positive or negative frequency offset and +x or −x RF phase. Application of a DC magnetic field pulse during one half of the t_1 period produces a net precession of ^{1}H polarization proportional to the field strength. ^{1}H NMR signals are detected with pulsed spin-locking (PSL), consisting of an RF pulse train with signal digitization in delays between the pulses. Cosine or sine modulations with respect to t_1 (*i.e.*, real or imaginary parts) are acquired by using either x or y RF phases in the PSL train.

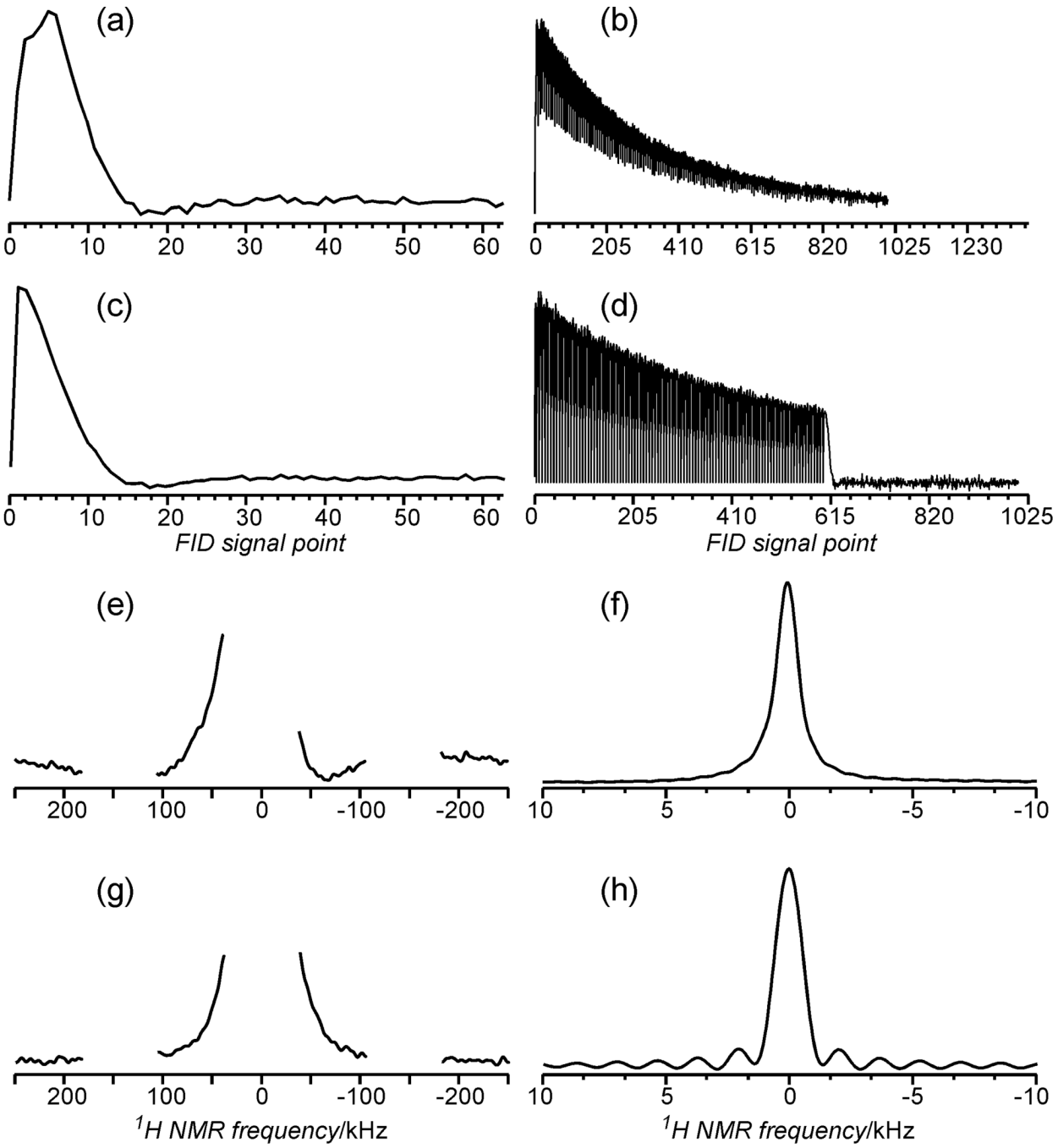

Figure 3.

Time-domain (a–d) and frequency-domain (e–h) ^{1}H NMR signals, either without (a,c,e,g) or with (b,d,f,h) pulsed spin-locking. Samples are 0.5 μl glycerol/water, either with 30 mM DOTOPA-TEMPO at 7 K (a,b,e,f) or with 5 mM DOTOPA-TEMPO at 35 K (c,d,g,h). FID signal points are digitized with a 1.0 μs dwell time, although points in (b) and (d) are not equally spaced due to the presence of RF pulses and ring-down delays in the PSL train (see text).

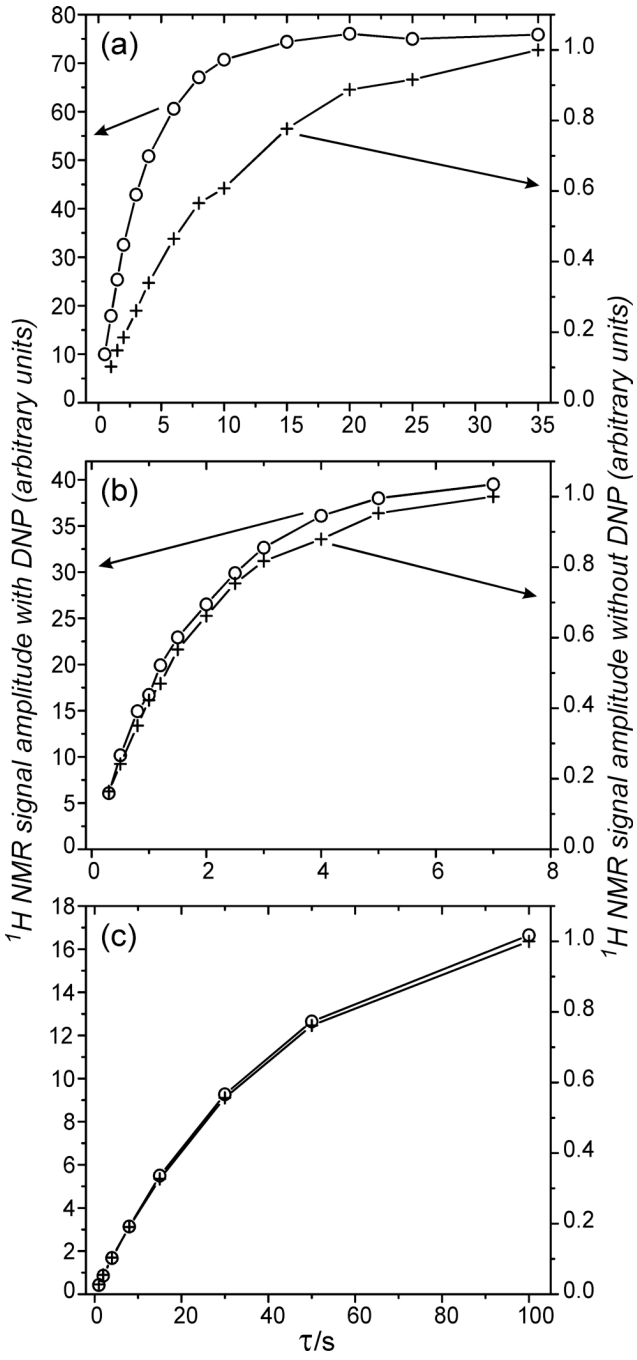

Figure 4.

Dependences of ^{1}H NMR signal amplitudes on the build-up time τ for glycerol/water with 30 mM DOTOPA-TEMPO at 7 K (a), 30 mM DOTOPA-TEMPO at 35 K (b), and 5 mM DOTOPA-TEMPO at 35 K (c). Data were obtained both with (circles, left axes) and without (crosses, right axes) microwave irradiation. In each panel, the signal amplitudes are scaled so that the largest signal without DNP has an amplitude equal to 1.0. Lines connecting data points are guides to the eye, not fits to theory or mathematical expressions.

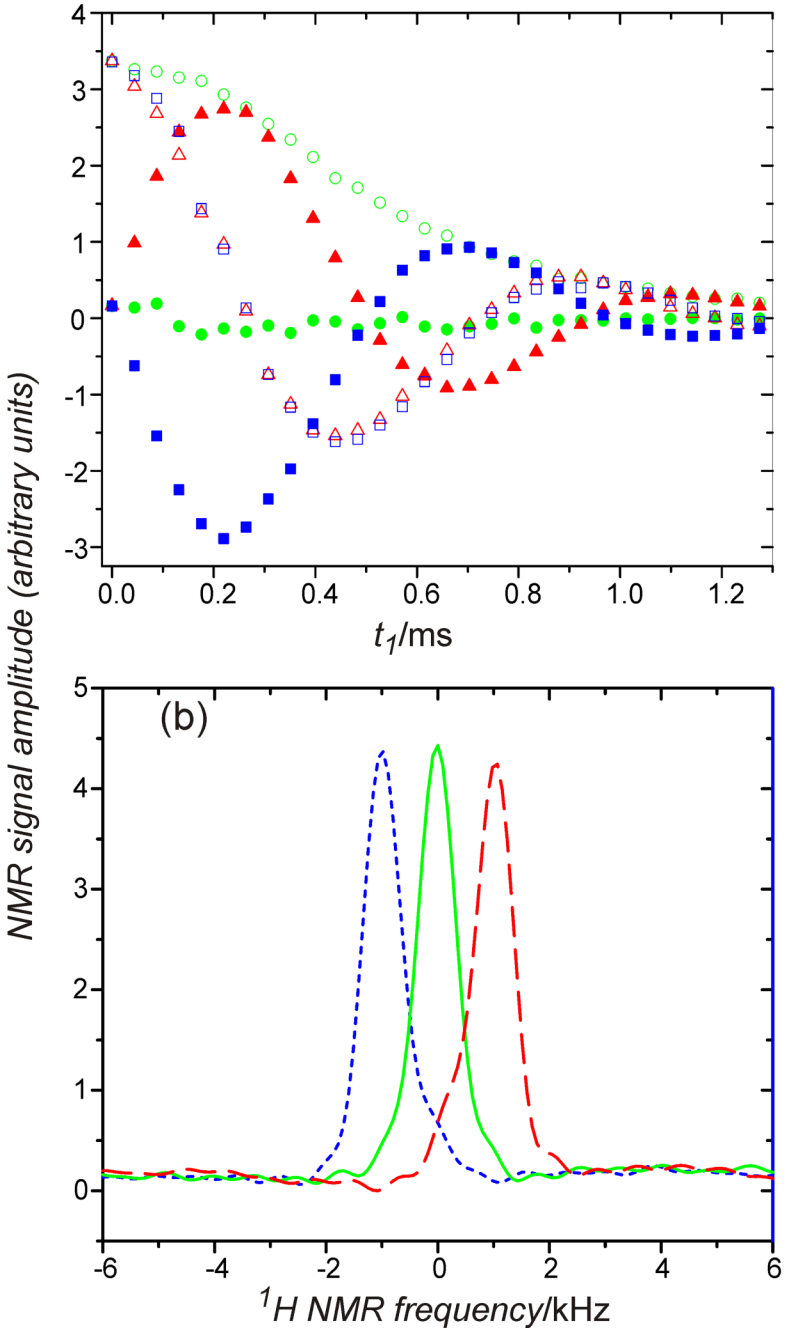

Figure 5.

(a) Dependences of ^{1}H NMR signal amplitudes on the Lee-Goldburg period t_1, for glycerol/water with 5 mM DOTOPA-TEMPO at 35 K. Real (hollow symbols) and imaginary (filled symbols) parts of the t_1 dependence are shown for experiments with DC field pulse amplitudes of 0.91, 0.0, and −0.91 G (squares, circles, and triangles, respectively). Lee-Goldburg decoupling conditions are described in the text. (b) Lineshapes obtained by Fourier transformation with respect to t_1 for 0.91, 0.0, and −0.91 G fields (short dashes, solid line, and long dashes, respectively)